Nanoscale

Rational design of guiding elements to control folding topology in i-motifs with multiple quadruplexes

Journal:	*Nanoscale*
Manuscript ID	NR-ART-01-2021-000611.R1
Article Type:	Paper
Date Submitted by the Author:	26-Mar-2021
Complete List of Authors:	Minasyan, Alexander; Northern Illinois University, Chemistry and Biochemistry Chakravarthy, Srinivas; Argonne National Laboratory Vardelly, Suchitra; Northern Illinois University, Chemistry and Biochemistry Joseph, Mark; University of Maryland Eastern Shore, Natural Sciences Nesterov, Evgueni; Northern Illinois University, Chemistry & Biochemistry; Louisiana State University, Chemistry Nesterova, Irina; Northern Illinois University, Department of Chemistry and Biochemistry

ARTICLE

Rational design of guiding elements to control folding topology in i-motifs with multiple quadruplexes

Received 00th January 20xx,
Accepted 00th January 20xx

DOI: 10.1039/x0xx00000x

Alexander S. Minasyan,[a] Srinivas Chakravarthy,[b] Suchitra Vardelly,[a] Mark Joseph,[c] Evgueni E. Nesterov,[a] and Irina V. Nesterova *[a]

Nucleic acids are versatile scaffolds that accommodate a wide range of precisely defined operational characteristics. Rational design of sensing, molecular computing, nanotechnology, and other nucleic acid devices requires precise control over folding conformations in these macromolecules. Here, we report a new approach that empowers well-defined conformational transitions in DNA molecular devices. Specifically, we develop tools for precise folding of multiple DNA quadruplexes (i-motifs) within the same oligonucleotide strand. To accomplish this task, we modify a DNA strand with kinetic control elements (hairpins and double stranded stems) that fold on a much faster timescale and consequently guide quadruplexes toward the targeted folding topology. To demonstrate that such guiding elements indeed facilitate formation of the targeted folding topology, we thouroughly characterize the folding/unfolding transitions through a combination of thermodynamic techniques, size exclusion chromatography (SEC) and small-angle X-ray scattering (SAXS). Furthermore, we extend SAXS capabilities to produce a direct insight on the shape and dimensions of the folded quadruplexes by computing their electron density maps from solution scattering data.

Introduction

Over the past two decades, nucleic acids have emerged as scaffolds for the design of nanomaterials with precisely defined functional characteristics.[1-8] A plethora of structural elements ranging from the conventional single stranded and antiparallel duplexes[9-12] to non-canonical triplexes,[13] quadruplexes,[14] parallel duplexes,[15-16] aptamers,[17] catalytic assemblies,[4] etc. contributes to the wealth of the material engineering capabilities. The ultimate success and proliferation of nucleic acids as a versatile nanotechnology platform is contingent upon continuing discovery, development, and characterization of the new functional capabilities of these scaffolds.

Nucleic acid quadruplexes as building blocks for nanoscale applications provide predictability of assembly, well characterized structural properties and high chemical, thermal, and mechanical stability.[14, 18] Thus, G-quadruplexes formed by guanine-rich sequences are principal components in functional structures ranging from highly stable 2D and 3D nano-assemblies[15] to analytical sensors[19] to therapeutic systems.[20] Cytosine-rich i-motif quadruplexes follow suit as nanotechnology tools,[14, 21-22] analytical sensors,[23-25] molecular logic operators[26], and smart drug delivery vehicles.[27] The advancement of those capabilities is dependent upon expansion of the toolbox for the fine control over precision folding in quadruplexes.

Recently, our group and others have focused on the unique sensing capabilities of i-motif quadruplexes. I-motifs are formed by cytosine-rich DNA strands that can function as multivalent receptors since their folding into quadruplexes is mediated by intercalated cytosine-proton-cytosine base pairs ($C\text{-}H^{+}\text{-}C$).[28-33] As scaffolds for sensing devices, i-motifs specifically benefit two areas: (i) sensors with the sharp response towards protons (also known as ultrasensitive sensors),[30-32, 34-38] and (ii) sensors based on molecular memory effects.[33] Engagement of multiple protons in the $C\text{-}H^{+}\text{-}C$ base pairing during i-motif's folding/unfolding empowers both capabilities: high positive cooperativity of the binding results in the ultrasensitive response while high entropic penalty enables the memory function.

Advancing either of these two sensing capabilities tools necessitates increasing the number of ligands (protons) participating in the i-motif folding/unfolding. However, design of such systems is intrinsically challenging as adding more $C\text{-}H^{+}\text{-}C$ pairs in the oligonucleotide strand results in a higher propensity towards formation of the kinetically trapped misfolded/partially folded species.[39-42] Therefore, full realization of the sensing capability is contingent upon the availability of the structural tools that deliberately minimize propensity of the i-motifs to form misfolded conformations. Also, understanding of folding pathways is also crucial for eliminating heterogeneity and imperfections in quadruplex folding, a major roadblock on the way of expanding the nanotechnological potential of nucleic acids.[14]

[a] Department of Chemistry and Biochemistry, Northern Illinois University, DeKalb, IL 60115, USA.
[b] X-ray Science Division, Argonne National Laboratory, Argonne, IL 60439, USA
[c] Department of Natural Science, University of Maryland Eastern Shore, Princess Anne, MD 21853, USA.

Electronic Supplementary Information (ESI) available: [details of any supplementary information available should be included here]. See DOI: 10.1039/x0xx00000x

ARTICLE

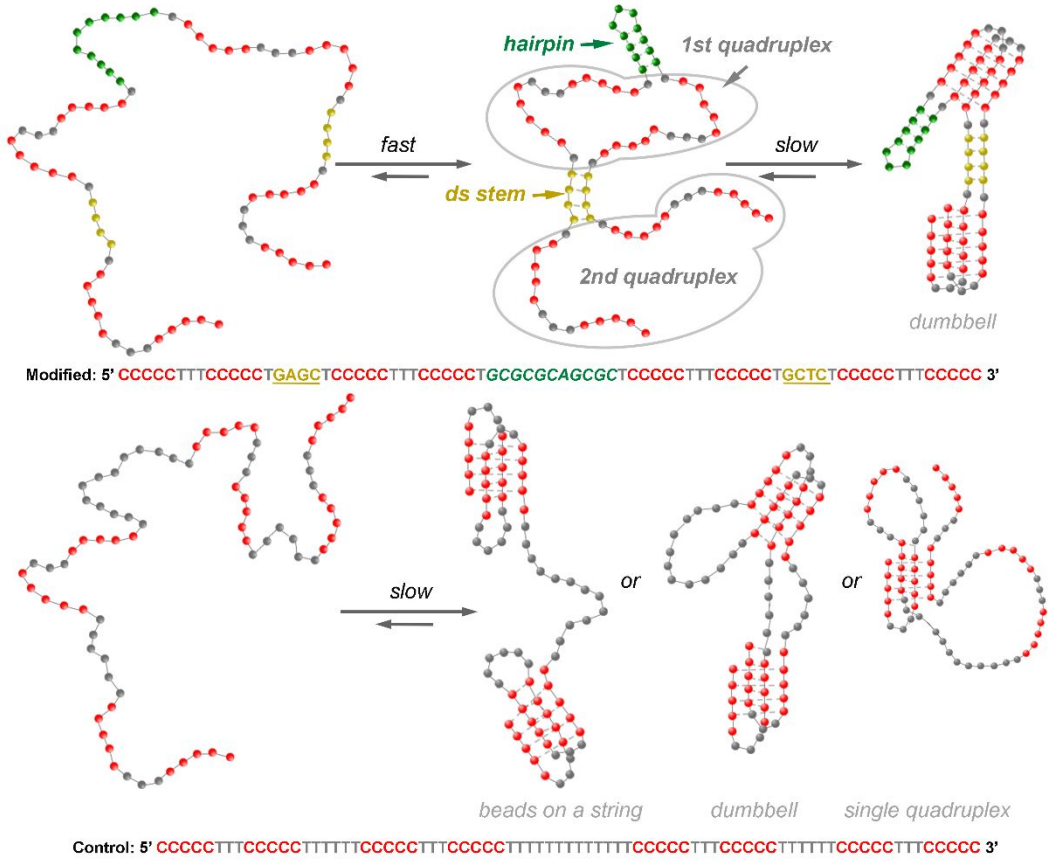

Figure 1. Folding pathways for an i-motif with two quadruplexes. An oligonucleotide strand with eight runs of cytosines (red) modified with two guiding elements – a hairpin (green) and double stranded stem (yellow) – folds into two discrete quadruplexes in a dumbbell pattern (top pathway). A control strand that is not modified with the guiding elements is likely to produce various misfolded conformations (bottom pathway). Bases participating in the formation of hairpin are italicized and green, double stranded stem – underlined and yellow, neutral thymidines are grey, cytosines – red.

In this work, we demonstrate a new structural approach that enables precise folding topology in i-motifs with an increasingly high number of C-H$^+$-C base pairs. To accomplish this goal, we engineer kinetic guiding elements that split large i-motifs into separate quadruplexes. We characterize the folded structure with the split quadruplexes and demonstrate the general utility of this approach.

Results and Discussion

As a model system, we design an i-motif with 20 potential C-H$^+$-C base pairs. The single stranded oligonucleotide includes eight runs of five cytosines interrupted with non-cytosines (Figure 1). One can envision a variety of conformations this structure can fold into, for example, "beads on a string" with consecutive cytosine runs forming two discrete quadruplexes, or a "dumbbell" conformation with the middle runs folding into a "head" quadruplex and the flanking runs folding into another quadruplex, or a mixed single quadruplex with participation of the different cytosine runs, etc. (some possible folded conformations are illustrated in Figure 1). In this work, we specifically target a "dumbbell" folding conformation consisting of the two discrete quadruplexes.

To achieve the "dumbbell" topology, we strategically design the non-cytosine bases to function as guiding elements that deliberately separate two quadruplexes. Antiparallel and parallel-stranded DNA fragments and hairpins have been previously documented to guide folding topology in some artificial G-quadruplex based systems[16, 43-49] and in a single i-motif quadruplex.[31] However, none of the previous reports explored guiding elements to simultaneously direct precise

folding of multiple quadruplexes of the same kind within the same strand. This is an intrinsically challenging task considering that such a system would show a higher propensity for forming misfolded conformations and intermolecular hybrids.

In our designed system, the two guiding elements are a hairpin and a double stranded stem (Figure 1). These elements fold on a much faster time scale compared to the quadruplexes: e.g. the rate constant (k_f) for a hairpin folding is on the order of 10^3-10^4 s^{-1},[50-52] whereas k_f for moderately large (five cytosines in a run) i-motifs is 10^{-4}-10^{-5} s^{-1}.[34, 53] Once folded, the guiding elements pre-arrange a targeted topology for a quadruplex. In our system, formation of a double stem is intended to split the strand into two quadruplexes, while the hairpin and the stem ensure optimized dumbbell folding topologies for the both i-motifs.

To design properly functioning guiding elements, we focus on: (i) relatively small hairpins and double stranded stems since those act as more efficient guiding elements[31]; (ii) hairpins and double stranded stems with high GC content as a necessary for efficient guiding;[31] (iii) minimizing probability of the non-target hybridization (e.g. no G-stretches that can hybridize C runs of i-motifs, and minimized complementarity between the stem of the hairpin and a double stranded guiding stem).

To contrast the effect of the guiding elements in the modified oligonucleotide, we study a control oligonucleotide that contains an identical sequence and distribution of the cytosine runs but does not incorporate the two guiding elements: both the stem and the hairpin are replaced with the stretches of thymidines that are incapable of duplex formation. Sequences for both oligonucleotides, modified and control, are included in Figure 1. To prove that the guiding elements indeed enable the targeted folding topology, we carefully studied and characterized folding of both modified and control structures through a combination of thermodynamic and structural techniques.

First, we investigate thermodynamic characteristics of the folding/unfolding transitions in the modified and control oligonucleotides. While thermodynamic studies do not yield folding topology, they do provide a critical support for proving our design concept. Specifically, we are looking for indications of a greater number of C-H$^+$-C bonds in the modified versus control oligonucleotide. Due to the guiding elements, both quadruplexes on the dumbbell are appropriately folded yielding the maximized number of C-H$^+$-C bonds. To derive the thermodynamic characteristics, we interrogate thermally induced folding/unfolding transitions of oligonucleotides. To exclusively focus on the i-motif transitions, we monitor UV absorbance at 295 nm where quadruplex folding/unfolding is visible but non-quadruplex transitions are inactive.[54-55]

Analysis of thermally induced folding/unfolding profiles (Figures 2A and S2, details in the ESI) consistently indicates the higher entropic and enthalpic contributions in folding of the modified oligonucleotide compared to the control (i.e. at pH 6.80 ΔH is –88 kcal mol^{-1} for modified vs. –57 kcal mol^{-1} for control; and ΔS is –288 cal mol^{-1} K^{-1} for modified vs. –188 cal mol^{-1} K^{-1} for control). Since C-H$^+$-C base pairing results in the negative changes in both enthalpy and entropy,[53] the observed trends

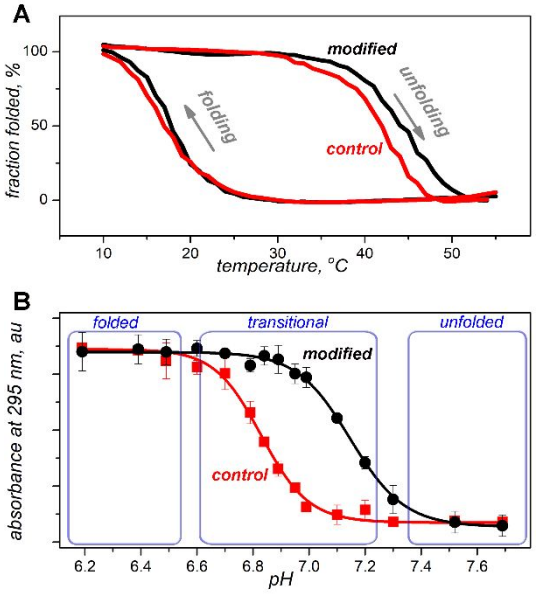

Figure 2. (A) thermal folding/unfolding profiles reflect higher stability of the modified (black trace) over control (red trace) i-motifs. The denaturations were acquired in 10 mM lithium cacodylate (pH 6.80) buffer at 0.2 °C/min cooling/heating rate. More experimental details are included in the ESI. (B) pH denaturation profile of the modified oligonucleotide (black circles) and the control (red squares). The profiles were acquired at room temperature using 500 nM samples equilibrated in PBS buffers. Error bars represent standard deviation of triplicate preparations of each sample.

are consistent with the greater number of C-H$^+$-C bonds formed upon folding of the modified oligonucleotide vs. control. Another key quantitative evidence of the higher number of C-H$^+$-C base pairs in the modified i-motif is the difference in the equilibrium melting temperature (T_m).[53, 56-59] For our system, we consistently observe a higher T_m for the modified oligonucleotide; for example, at pH 6.80 equilibrium T_m is 30.7 °C for the modified vs. 28.6 °C for the control (Figures 2A and S3). We observe similar trends in the T_m, ΔH, and ΔS in the buffers with other pH values (e.g. at pH 6.70, Figures S2 and S4, experimental procedures in the ESI).

We draw further evidence on the higher number of C-H$^+$-C pairs in the modified oligonucleotide from the analysis of hysteresis loops on the thermal denaturation profiles. Slow entropy-limited folding is one of the major contributors to the thermal hysteresis in multivalent structures.[60-61] The higher entropic contribution, in turn, originates from the higher number of the C-H$^+$-C base pairs actually formed. Therefore, the wider hysteresis loops should correlate with a larger number of the C-H$^+$-C pairs. Indeed, as it was demonstrated for a range of i-motifs, participation of a higher number of the C-H$^+$-C pairs does tend to exhibit wider hysteresis loops.[53, 56, 58, 62] In our system, we consistently observe wider hysteresis loops (ΔT_m) for the modified compared to the control oligonucleotide. Thus, at pH 6.80, ΔT_m for the modified oligonucleotide is 26.9 °C vs. 24.7 °C for the control (Figure 2A); at pH 6.70 ΔT_m is 22.3 °C for the modified vs. 21.3 °C for the control (Figure S2). The consistent observations of the wider hysteresis loops for the modified oligonucleotides support greater number of the C-H$^+$-C pairs in the modified i-motif compared to the control.

In order to establish the range for the conformational changes occurring under isothermal conditions, we evaluate pH denaturation profiles for both oligonucleotides. In agreement with the previous reports that hairpins inside the i-motif loops stabilize the quadruplex structure,[31, 34, 63] we observe increased stability of the modified oligonucleotide compared to the control (Figure 2B) Based on the profiles, we derive information on a distribution of the folded and unfolded conformations over a pH range: thus, at pH 6.4 both oligonucleotides are folded, at pH 7.6 both are unfolded, and pH's 6.8 and 7.0 represent some transitional points.

To gain a direct insight on the i-motifs' folding topology and conformational transitions, we take advantage of the size exclusion chromatography (SEC) – small-angle X-ray scattering (SAXS) combination. SAXS is a powerful technique that enables direct characterization of the dimensions and shape of macromolecules in solution, including oligonucleotides.[64] With respect to i-motifs in solution, SAXS can differentiate not only between folded and unfolded forms[65] but also between fully and partially-folded conformations [66]. However, as a technique that probes the shape and dimensions of the molecules in a bulk sample, SAXS results can be obscured by the presence of intermolecular hybrids and aggregated states. At the high (50 µM and above) concentrations required for SAXS, our oligonucleotides may be highly susceptible to intermolecular binding: e.g. we would expect a higher probability of forming self-dimers with complementary base pairing of the hairpin and double stranded stems, and/or intermolecular i-motifs, and/or higher-order aggregates mediated by the C-H$^+$-C base pairing. As a result, SAXS data on a mixture of aggregated, partially aggregated, and non-aggregated components in solution would be rather meaningless and could not be used to decipher structural information on the individual components. Therefore, upfront SEC separation is crucial to ensure that the acquired SAXS data exclusively represent the non-aggregated intramolecular folds. In addition, SEC yields a valuable information *per se*: the technique not only differentiates between the folded and unfolded quadruplexes but also hints

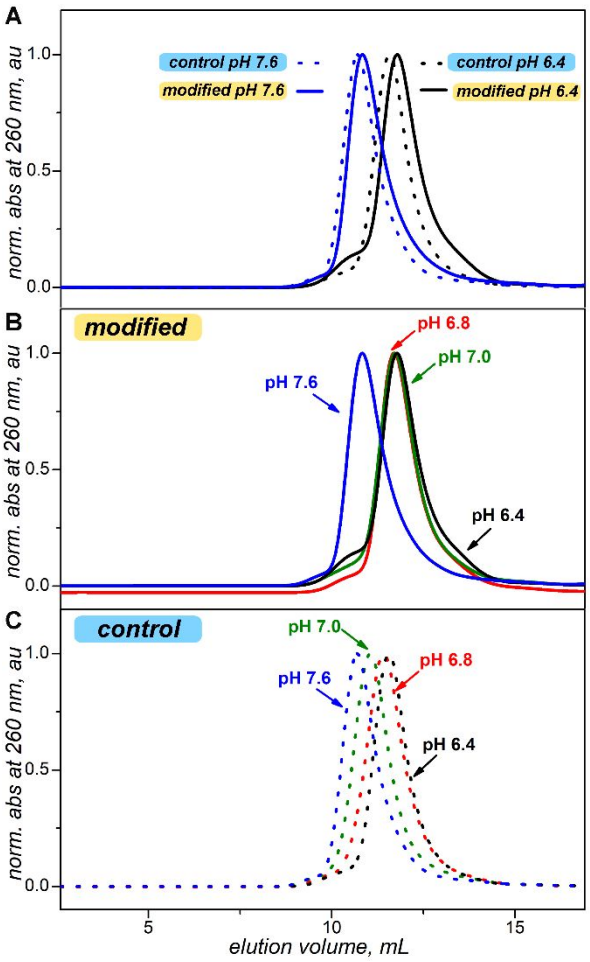

Figure 3. SEC profiles (UV detection) of the modified and control oligonucleotides at various pH. (A) A clear difference in elution volume is observed between folded (pH 6.4) and unfolded (pH 7.6) conformations for each oligonucleotide. In addition, a small difference in elution volume between the modified and control oligonucleotides at both pH values conforms to the design consideration that both folded and unfolded conformations of the modified oligonucleotide are more compact (i.e. correspond to a higher elution volume). (B) Modified oligonucleotide transitions from an unfolded to folded conformation within a pH range 7.0-7.6 with no intermediate states detected, whereas transition of the control oligonucleotide proceeds gradually over a wider pH range of 6.4-7.6 through a series of clearly differentiated intermediate states (C). The separations were performed on approx. 50 µM samples using Superdex 75 column and PBS buffers with properly adjusted pH's as a mobile phase.

on relative compactness of the folded structures. Thus, Largy and Mergny previously demonstrated[67] that for a given molecular weight, a quadruplex-forming oligonucleotide showing a higher retention time has a smaller hydrodynamic volume and can be considered more compact.

As expected, SEC indeed effectively differentiates between folded and unfolded conformations of the modified and control oligonucleotides (Figure 3). The SEC profiles for the presumably folded (pH 6.4) and unfolded (pH 7.6) structures for both oligonucleotides are well separated: elution volumes at pH 6.4 (folded) are smaller than those at pH 7.6 (unfolded). Furthermore, we consistently observe difference in the elution volume for folded conformations of the two different oligonucleotides (pH 6.4, Figure 3A). This difference confirms

the design consideration that the modified oligonucleotide possesses a more compact folded conformation and, therefore, is retained longer. We also notice a slightly more compact conformation of the unfolded (pH 7.6) modified oligonucleotide in comparison to the control: the difference likely originates from the presence of hybridized hairpin and stem in the modified oligonucleotide.

In the SEC/SAXS setup, a sample solution is flowed through a SAXS cell directly after exiting from the SEC column; the scattering data *I(q)* corresponding to the peaks on the SEC elution profiles are used for further analysis (Figure 4A, B). Evaluation of the SAXS data provides a direct insight into aggregation state, size, shape, and compactness of the modified and control

ARTICLE

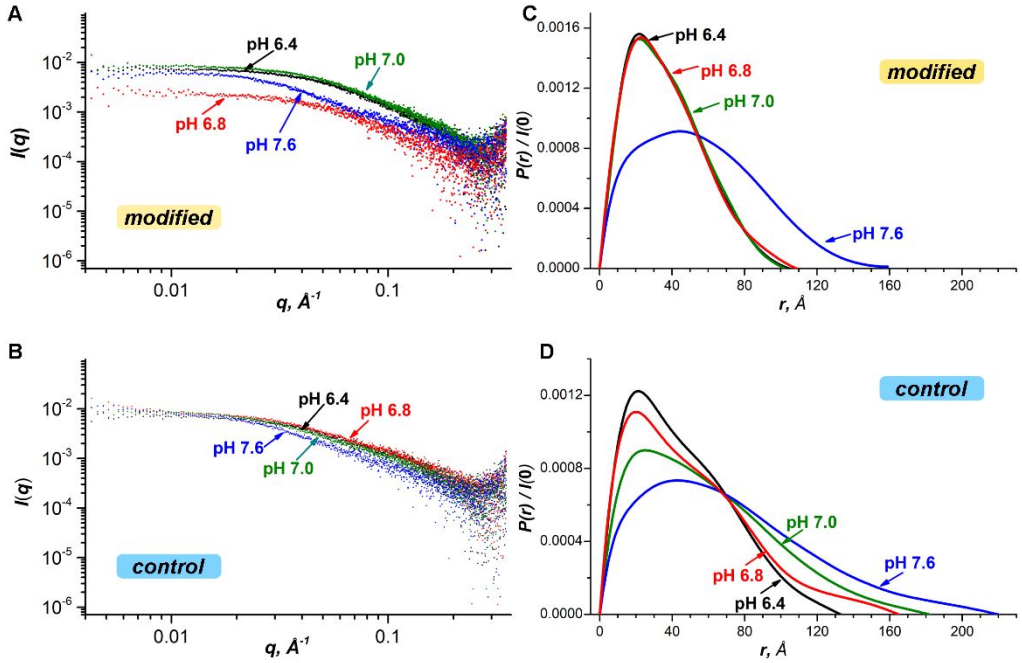

Figure 4. Original scattering data *(I(q)* vs. *q*) for modified (A) and control (B) oligonucleotides. Normalized pair distance distribution function (*P(r)/I(0)*) derived from the scattering data clearly indicates more compact shape of the modified oligonucleotide (C) compared to the control (D) over the whole pH range.

Table 1. Values for R_g and D_{max} derived from *P(r)* function analysis and, independently, from analysis of the Guinier plots.

pH	R_g, Å				D_{max}, Å	
	Modified		Control		Modified	Control
	P(r) analysis	Guinier plot	*P(r)* analysis	Guinier plot	*P(r)* analysis	*P(r)* analysis
6.4	29.7	28.7	37.2	35.1	105	133
6.8	30.2	28.5	42.4	36.4	109	165
7.0	29.9	29.1	48.8	45.0	102	182
7.6	45.3	44.5	59.6	53.3	159	220

oligonucleotides in solution at different pH values. The analysis of the Guinier region at low *q* allows both evaluating the quality of the scattering data and checking for the presence of undesired aggregated species. The linearity of the Guinier fit (ln[*I(q)*] vs. q^2, Figure S1 in the ESI) in the entire low-*q* region supports predominant scattering from the non-aggregated species whereas a characteristic upturn in the Guinier plot at low *q* indicates presence of the aggregates in the scattering solution.[68] The analysis of the experimental data in Figure S1 reveals no aggregate presence for the modified oligonucleotide within the entire pH range, and for the control oligonucleotide at pH 6.4 and 6.8 (and possibly some but ameliorable aggregation at pH 7.0 and 7.6). The Guinier fit is also used to obtain radius of gyration (R_g), the average root-mean-square distance from the center of density (Table 1), that reflects both the size and conformational/folding state of the modified and control oligonucleotides.

The inverse Fourier transform of the scattering data *I(q)* produces a pair distance distribution function *P(r)* which represents the histogram of distance distributions within the oligonucleotide (Figure 4 C and D). The *P(r)* function yields two critical parameters directly reflecting an i-motif folding topology: radius of gyration (R_g), and the maximum linear dimension of the i-motif molecule (D_{max}), as shown in Table 1. Since the R_g values obtained from *P(r)* function come from the analysis of the entire *I(q)* scattering curve, they are potentially more reliable than the R_g values obtained from the low-*q* Guinier fit. Both R_g and D_{max} are direct measures of the oligonucleotide size and reflect its conformational state.[69] In order to account for the concentration variations in the SEC/SAXS setup, Figure 4C, D shows normalized *P(r)/I(0)* pair distance distribution function curves, that are adjusted by the forward scattering intensity *I(0)*. The shape of the *P(r)* functions provides some substantial information on the shape and dimensions of the biomacromolecules in solution.[70]

Specifically, the modified oligonucleotide is characterized by the nearly similar *P(r)* functions at the three pH values (6.4, 6.8 and 7.0) and a distinctly different function at the pH 7.6 (Figure 4C). On the other hand, there is a continuous change in the shape of the *P(r)* function upon increasing pH for the control oligonucleotide (Figure 4D). This observation directly demonstrates that the modified oligonucleotide mostly retains its compact folded conformation within the pH range of 6.4-7.0, and transitions to an unfolded conformation at pH 7.6. The control oligonucleotide transitions from a folded (at pH 6.4) to an unfolded (at pH 7.6) conformations within a broader pH range, with some intermediate (partially unfolded) conformations involved in the process. This highlights the unique role of the designed guiding elements in the modified oligonucleotide in imposing control over its sharp conformational transition.

Further analysis of the *P(r)* plots and the R_g and D_{max} data (Figure 4C, D and Table 1) reveals that the modified oligonucleotide possesses a more compact folded conformation compared to the control. Thus, at pH 6.4 where both structures are folded, R_g of the modified oligonucleotide is 29.7 Å while it is 37.2 Å for the control. Maximum linear dimension, D_{max}, values also follow the same trend: for the modified oligonucleotide D_{max} is 105 Å vs. 133 Å for the control. In excellent agreement with the SEC data, we observe that the modified oligonucleotide is also more compact in its unfolded state (at pH 7.6, R_g = 45.3 Å) compared to the control (R_g = 59.6 Å at pH 7.6). As mentioned above, this difference may originate from the presence of a hairpin and a double stranded stem in the modified oligonucleotide that keep its structure more compact.

Comparison of the R_g values obtained using Guinier fit and determined directly from the *P(r)* function can also provide some information on the biomacromolecular structure. Typically, for compact, tightly folded systems, the R_g values from both methods should agree well (as is the case for the modified oligonucleotide, Table 1). On the other hand, it has been observed that for less tightly folded (i.e. more disordered and more flexible) systems, R_g values derived from *P(r)* function tend to be characteristically larger than the R_g values obtained from the Guinier fit.[69] This indeed is observed for the control oligonucleotide (Table 1). This highlights the tighter and more well-defined structure of the folded conformation of the modified oligonucleotide.

Over the years, SAXS has evolved into a powerful tool that can provide not only some information on general shape and dimensions of biomacromolecules but also can be used to produce reconstructed low-resolution structural images of the complex biopolymers. A recently developed DENSS algorithm applies an iterative structure factor retrieval procedure to experimental scattering data to generate *ab initio* electron density maps of complex macromolecular structures in solution.[71] The major advantage of this algorithm over other, more traditional shape-reconstruction models is that it captures non-uniform molecular volumes and detects differences in dissimilar electron densities, therefore it can be applied even to relatively disordered or multi-domain systems.[72-74] Using DENSS algorithm, we, for the first time, reconstruct molecular shapes of the folded states of the modified and control oligonucleotides (Figure 5). The reconstructed electron density maps of the modified oligonucleotide show an excellent agreement with our structural design. Particularly, the folded conformation features two distinct i-motif domains that are twisted with respect to each other. Importantly, the reconstructed molecular shapes clearly show that both i-motifs in the modified oligonucleotide fold in more compact, dense and less spatially spread structures compared to the control oligonucleotide – providing an excellent support to our structural design and agreeing well with the other experimental observations discussed above. It is harder to define precise shape of a folded conformation of the control oligonucleotide based on the low-resolution electron density reconstruction; however, we speculate that the electron density surface may indicate preference for the "beads-on-the-string" topology with the less densely folded i-motif fragments.

In order to expand the scope on the new approach and demonstrate its generality, we designed another, even more compact, double-quadruplex structure (Figure S5 in the ESI) designated as *modified*^{TS}. The new structure does not possess a head hairpin but has two short double stranded stems that intend to guide folding of the two discrete quadruplexes. We preliminary characterized *modified*^{TS} and the corresponding control (*control*^{TS}) using SEC/SAXS. As envisioned in the design, (i) the *modified*^{TS} is more compact in the folded conformation than *control*^{TS}: R_g and D_{max} for *modified*^{TS} are 28.3 Å and 98 Å, respectively, vs. 39.1 Å and 142 Å for *control*^{TS}; (ii) *modified*^{TS} is more compact than *modified* oligonucleotide in Figure 1; thus, R_g and D_{max} for the folded *modified*^{TS} are 28.3 Å and 98 Å respectively (pH 6.70) vs. 30.2 Å and 109 Å (pH 6.80) for the folded *modified*. The results correlate with an expectation that the "two-stem" ("TS") series are more compact as a hairpin is replaced with a stem. Complete characterization of the "TS" structures is summarized in Figures S5-S8 and Table S1 in the ESI. Overall, our data clearly indicate that guiding elements enable precise and effective programmable engineering of oligonucleotide nanostructures.

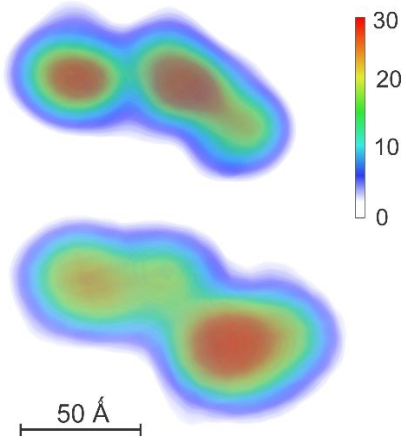

Figure 5. Electron density reconstruction of the folded conformations of the modified (top) and control (bottom) oligonucleotides in solution at pH 6.4. The maps were

obtained using the DENSS algorithm based on the corresponding experimental scattering data, the electron densities are shown as volumes colored according to density (a color bar indicates electron density in the units of σ). The estimated resolution for the reconstructions is 28 Å for the modified and 26 Å for the control oligonucleotide.

Conclusions

For the first time, we demonstrate that modifying oligonucleotides with properly designed guiding elements enables precise control over the folding topology of multiple quadruplexes within the same molecular system. Our conclusions are supported by the combination of classical thermodynamic and advanced structural tools. With respect to structural characterization, we demonstrate that a SEC/SAXS setup is a powerful experimental approach for direct insight into structural morphology and shape of the folded and unfolded oligonucleotide conformations. Applying the computational DENSS algorithm to the SEC/SAXS data enables reconstructing electron density surfaces and characterizing actual shapes of the intramolecularly folded double quadruplex oligonucleotides in solution.

The ability to exert significant control over conformational transitions in oligonucleotides will provide an effective tool for the design of DNA-based molecular devices, a crucial asset for the field of DNA nanotechnology. In general, the ability to generate homogeneous populations of precisely folded structures is a key to full realization of nanotechnological capabilities of nucleic acids. The reported findings are very encouraging for our ongoing efforts to develop sensing systems with high positive binding cooperativity or molecular memory.

While this proof-of-concept demonstration was performed with i-motif quadruplexes, we expect that similar design principles will be applicable to other molecular structures when a precise folding topology is targeted. Moreover, amid recent discoveries of i-motifs existing inside living cells,[28, 75-77] these findings will contribute towards understanding of folding pathways of various quadruplexes within complex landscapes of genomic DNA and RNA.[78]

Author Contributions

A.S.M., M.J. and S.V. designed the methodology, performed spectroscopic experiments and analyzed and discussed the data. S.C. carried out SEC/SAXS experiments and data reduction; E.E.N. performed detailed SAXS data analysis and computational studies. I.V.N. produced an original idea of this work, designed the general experimental methodology, and supervised the project. All authors contributed to the discussion of this manuscript and its writing.

Conflicts of interest

Authors declare no conflicts of interest.

Acknowledgements

Research reported in this publication was supported by the National Institute of General Medical Sciences of the National Institutes of Health under Award Number R15GM135796. This research used resources of the Advanced Photon Source, a U.S. Department of Energy (DOE) Office of Science User Facility operated for the DOE Office of Science by Argonne National Laboratory under Contract No. DE-AC02-06CH11357. We extend gratitude to Mr. Zane LaCasse (Northern Illinois University) for his help with SEC/SAXS experiments. We also thank Professor Gerald J. Schneider and Dr. Sudipta Gupta (Louisiana State University) for the helpful discussions on SAXS studies.

Notes and references

1 J. Lee, L. Lin and Y. Li, Functional Nucleic Acids for Fuorescence-Based Biosensing Applications. In *Advanced Fluorescence Reporters in Chemistry and Biology III: Applications in Sensing and Imaging*, Demchenko, A. P., Ed. Springer GmbH: 2011; Vol. 10, pp 201-221.

2 Y. Krishnan and F. C. Simmel, *Angew. Chem., Int. Ed.,* 2011**, 50**.

3 M. Xiao, W. Lai, T. Man, B. Chang, L. Li, A. R. Chandrasekaran and H. Pei, *Chem. Rev. ,* 2019**, 119**, 11631.

4 E. M. McConnell, I. Cozma, D. Morrison and Y. Li, *Anal. Chem.,* 2020**, 92**, 327.

5 S. Ranallo, A. Porchetta and F. Ricci, *Anal. Chem.,* 2019**, 91**, 44.

6 K. Chakraborty, A. T. Veetil, S. R. Jaffrey and Y. Krishnan, *Annu. Rev. Biochem.,* 2016**, 85**, 349.

7 S. G. Harroun, C. Prévost-Tremblay, D. Lauzon, A. Desrosiers, X. M. Wang, L. Pedro and A. Vallée-Bélisle, *Nanoscale,* 2018**, 10**, 4607.

8 F. Wang, X. Liu and I. Willner, *Angew. Chem., Int. Ed.,* 2015**, 54**, 1098.

9 S. Thekkan, M. S. Jani, C. Cui, K. Dan, G. L. Zhou, L. Becker and Y. Krishnan, *Nat. Chem. Biol.,* 2019**, 15**, 1172.

10 M. S. Jani, J. Y. Zou, A. T. Veetil and Y. Krishnan, *Nat. Chem. Biol.,* 2020**, 16**, 660.

11 A. T. Veetil, J. Zou, K. W. Henderson, M. S. Jani, S. M. Shaik, S. S. Sisodia, M. E. Hale and Y. Krishnan, *Proc. Natl. Acad. Sci. U. S. A.,* 2020**, 117**, 14694.

12 D. M. Kolpashchikov, *Acc. Chem. Res.,* 2019**, 52**, 1949.

13 Y. Hu, A. Cecconello, A. Idili, F. Ricci and I. Willner, *Angew. Chem., Int. Ed.,* 2017**, 56**, 15210.

14 J.-L. Mergny and D. Sen, *Chem. Rev. ,* 2019**, 119**, 6290.

15 L. A. Yatsunyk, O. Mendoza and J.-L. Mergny, *Acc. Chem. Res.,* 2014**, 47**, 1836.

16 L. A. Yatsunyk, O. Piétrement, D. Albrecht, P. L. T. Tran, D. Renčiuk, H. Sugiyama, J. M. Arbona, J. P. Aimé and J. L. Mergny, *ACS Nano,* 2013**, 7**, 5701.

17 Y. Wu, I. Belmonte, K. S. Sykes, Y. Xiao and R. J. White, *Anal. Chem.,* 2019**, 91**.

18 B. Kankia, *J. Phys. Chem. B,* 2014**, 118**, 6134.

19 H. Y. Peng, A. M. Newbigging, Z. X. Wang, J. Tao, W. C. Deng, X. C. Le and H. Q. Zhang, *Anal. Chem.,* 2018**, 90**, 190.

20 P. J. Bates, E. M. Reyes-Reyes, M. T. Malik, E. M. Murphy, M. G. O'Toole and J. O. Trent, *Biochim. Biophys. Acta, Gen. Subj.,* 2017**, 1861**, 1414.

21 Y. C. Dong, Z. Q. Yang and D. S. Liu, *Acc. Chem. Res.,* 2014**, 47**, 1853.

22 T. Li and M. Famulok, *J. Am. Chem. Soc.,* 2013**, 135**, 1593.

23 A. Dembska, P. Bielecka and B. Juskowiak, *Anal. Methods,* 2017**, 9**, 6092.

24 J. J. Alba, A. Sadurní and R. Gargallo, *Crit. Rev. Anal. Chem.,* 2016**, 46**, 443.
25 A. Dembska, *Anal. Chim. Acta,* 2016**, 930**, 1.
26 M. Wang, G. X. Zhang and D. Q. Zhang, *Chem. Commun.,* 2015**, 51**, 3812.
27 C. E. Chen, F. Pu, Z. Z. Huang, Z. Liu, J. S. Ren and X. G. Qu, *Nucleic Acids Res.,* 2011**, 39**, 1638.
28 H. A. Assi, M. Garavís, C. González and M. J. Damha, *Nucleic Acids Res.,* 2018**, 46**, 8038.
29 S. Benabou, A. Aviño, R. Eritja, C. González and R. Gargallo, *RSC Adv.,* 2014**, 4**, 26956.
30 Z. LaCasse, J. R. Briscoe, E. E. Nesterov and I. V. Nesterova, *Anal.Chem.,* 2019**, 91**, 14275.
31 I. V. Nesterova, J. R. Briscoe and E. E. Nesterov, *J. Am. Chem. Soc.,* 2015**, 137**, 11234.
32 I. V. Nesterova and E. E. Nesterov, *J. Am. Chem. Soc.,* 2014**, 136**, 8843.
33 O. A. Nwokolo, B. Kidd, T. Allen, A. S. Minasyan, S. Vardelly, K. D. Johnson and I. V. Nesterova, *Angew. Chem., Int. Ed.,* 2021**, 60**, 1610.
34 I. V. Nesterova, S. O. Elsiddieg and E. E. Nesterov, *J. Phys. Chem. B.,* 2013**, 117**, 10115.
35 X. Hua, E. Yang, W. Yang, R. Yuan and W. Xu, *Chem. Commun.,,* 2019**, 55**, 12463.
36 Y. Lei, X. He, J. Tang, H. Shi, D. He, L. a. Yan, J. Liu, Y. Zeng and K. Wang, *Chem. Commun.,* 2018**, 54**, 10288.
37 W. Ma, L. a. Yan, X. He, T. Qing, Y. Lei, Z. Qiao, D. He, K. Huang and K. Wang, *Anal. Chem.,* 2018**, 90**, 1889.
38 S. Halder and Y. Krishnan, *Nanoscale,* 2015**, 7**, 10008.
39 M. A. Mullen, S. M. Assmann and P. C. Bevilacqua, *J. Am. Chem. Soc.,* 2012**, 134**, 812.
40 S. Dhakal, J. L. Lafontaine, Z. B. Yu, D. Koirala and H. B. Mao, *PLoS One,* 2012**, 7**, e39271.
41 S. Dhakal, J. D. Schonhoft, D. Koirala, Z. B. Yu, S. Basu and H. B. Mao, *J. Am. Chem. Soc.,* 2010**, 132**, 8991.
42 S. M. Reilly, D. F. Lyons, S. E. Wingate, R. T. Wright, J. J. Correia, D. M. Jameson and R. M. Wadkins, *Biophys. J.,* 2014**, 107**, 1703.
43 K. W. Lim, Z. J. Khong and A. T. Phan, *Biochemistry,* 2014**, 53**.
44 K. W. Lim and A. T. Phan, *Angew. Chem., Int. Ed.,* 2013**, 52**.
45 J. Zhou, A. Bourdoncle, F. Rosu, V. Gabelica and J. L. Mergny, *Angew. Chem., Int. Ed.,* 2012**, 51**.
46 Y. C. Huang and D. Sen, *Angew. Chem., Int. Ed.,* 2014**, 53**.
47 O. Mendoza, M. Porrini, G. F. Salgado, V. Gabelica and J.-L. Mergny, *Chem. Eur. J.,* 2015**, 21**, 6732.
48 T. Q. N. Nguyen, K. W. Lim and A. T. Phan, *Nucleic Acids Res.,* 2020**, 48**, 10567.
49 T. Q. N. Nguyen, K. W. Lim and A. T. Phan, *J. Phys. Chem. B,* 2020**, 124**, 5122.
50 G. Bonnet, O. Krichevsky and A. Libchaber, *Proc. Natl. Acad. Sci. U.S.A.,* 1998**, 95**.
51 M. I. Wallace, L. Ying, S. Balasubramanian and D. Klenerman, *J. Phys. Chem. B,* 2000**, 104**.
52 Y. Shen, S. V. Kuznetsov and A. Ansari, *J. Phys. Chem. B,* 2001**, 105**.
53 J. L. Mergny and L. Lacroix, *Nucleic Acids Res.,* 1998**, 26**, 4797.
54 J. L. Mergny and L. Lacroix, *Oligonucleotides,* 2003**, 13**, 515.
55 P. A. Rachwal and K. R. Fox, *Methods,* 2007**, 43**, 291.
56 E. P. Wright, J. L. Huppert and Z. A. E. Waller, *Nucleic Acids Res.,* 2017**, 45**, 2951.
57 A. M. Fleming, Y. Ding, R. A. Rogers, J. Zhu, J. Zhu, A. D. Burton, C. B. Carlisle and C. J. Burrows, *J. Am. Chem. Soc.,* 2017**, 139**, 4682.
58 R. A. Rogers, M. R. Meyer, K. M. Stewart, G. M. Eyring, A. M. Fleming and C. J. Burrows, *Biopolymers,* 2020, DOI: 10.1002/bip.23389.
59 P. Školáková, D. Renčiuk, J. Palacký, D. Krafčík, Z. Dvořáková, I. Kejnovská, K. Bednářová and M. Vorlíčková, *Nucleic Acids Res.,* 2019**, 47**, 2177.
60 M. Shigeno, Y. Kushida and M. Yamaguchi, *ChemPhysChem,* 2015**, 16**, 2076.
61 M. Shigeno, Y. Kushida and M. Yamaguchi, *Chem. Commun.,* 2016**, 52**, 4955.
62 J. L. Mergny, *Biochemistry,* 1999**, 38**, 1573.
63 S. Benabou, R. Ferreira, A. Aviñó, C. González, S. Lyonnais, M. Solà, R. Eritja, J. Jaumot and R. Gargallo, *Biochim. Biophys. Acta, Gen. Subj.,* 2014**, 1840**.
64 P. W. Wu, Y. Yu, C. E. McGhee, L. H. Tan and Y. Lu, *Adv. Mater.,* 2014**, 26**, 7849.
65 K. S. Jin, S. R. Shin, B. Ahn, S. Jin, L. Rho, H. Kim, S. J. Kim and M. Ree, *J. Phys. Chem. B,* 2010**, 114**, 4783.
66 K. S. Jin, S. R. Shin, B. Ahn, Y. Rho, S. J. Kim and M. Ree, *J. Phys. Chem. B,* 2009**, 113**, 1852.
67 E. Largy and J. L. Mergny, *Nucleic Acids Res.,* 2014**, 42**, e149.
68 D. A. Jacques and J. Trewhella, *Protein Sci.,* 2010**, 19**, 642.
69 A. G. Kikhney and D. I. Svergun, *FEBS Lett.,* 2015**, 589**, 2570.
70 D. I. Svergun and M. H. J. Koch, *Rep. Prog. Phys.,* 2003**, 66**, 1735.
71 T. D. Grant, *Nat. Methods,* 2018**, 15**, 191.
72 C. A. Brosey and J. A. Tainer, *Curr. Opin. Struct. Biol.,* 2019**, 58**, 197.
73 D. Srivastava and N. O. Artemyev, *J. Biol. Chem.,* 2019**, 294**, 1785.
74 J.-H. Shin, A. G. Sulpizio, A. Kelley, L. Alvarez, S. G. Murphy, L. X. Fan, F. Cava, Y. X. Mao, M. A. Saper and T. Dörr, *Proc. Natl. Acad. Sci. U. S. A.,* 2020**, 117**, 11692.
75 S. Dzatko, M. Krafcikova, R. Hansel-Hertsch, T. Fessl, R. Fiala, T. Loja, D. Krafcik, J. L. Mergny, S. Foldynova-Trantirkova and L. Trantirek, *Angew. Chem., Int. Ed.,* 2018**, 57**, 2165.
76 M. Zeraati, D. B. Langley, P. Schofield, A. L. Moye, R. Rouet, W. E. Hughes, T. M. Bryan, M. E. Dinger and D. Christ, *Nat. Chem.,* 2018**, 10**, 631.
77 H. Abou Assi, M. Garavís, C. González and M. J. Damha, *Nucleic Acids Res.,* 2018**, 46**, 8038.
78 D. Varshney, J. Spiegel, K. Zyner, D. Tannahill and S. Balasubramanian, *Nat. Rev. Mol. Cell Biol.,* 2020**, 21**, 459.